Anbar Journal of Engineering Science (AJES) **Vol. 16 , No. 2 (2025) , pp. 87 ~ 101**
P-ISSN: 1997-9428 ; E-ISSN: 2706-7440 DOI: http://doi.org/10.37649/AJES-25-006

University of Anbar

Anbar Journal of Engineering Science

journal homepage: https://ajes.uoanbar.edu.iq/

Numerical and Experimental Investigations on Hydrothermal Characteristics of Turbulent Flow in Channel with Circular Turbulators

Albashir A. Obeid[a]*, M. A. Ahmed[b], Mohd Zamri Yusoff[c]

[a]*Department of Mechanical Engineering, College of Engineering, University of Anbar, Ramadi, 31001, Anbar, Iraq.*
Email:alb22e2002@uoanbar.edu.iq , https://orcid.org/0009-0005-2397-1525

[b]*Department of Mechanical Engineering, College of Engineering, University of Anbar, Ramadi, 31001, Anbar, Iraq.*
Email:mohammed.abed@uoanbar.edu.iq , https://orcid.org/0000-0003-0598-6895

[c]*Department of Mechanical Engineering, Universiti Tenaga Nasional, Kajang, Selangor, Malaysia, TNB Research Sdn. Bhd., Kajang, Selangor.*
mohdzamri.yusoff@tnb.com.my , https://orcid.org/0000-0003-0568-6345

PAPER INFO

Paper history
Received: 03/07/2025
Revised: 12/10/2025
Accepted: 19/11/2025

Keywords:
Circular turbulators
Turbulence phenomena
Finite volume approach
Adiabatic turbulators

ABSTRACT

In this study, turbulent flow and heat transfer in a two-dimensional channel equipped with adiabatic circular turbulators were investigated both experimentally and numerically for Reynolds numbers of 2000, 3000, 4000, and 5000. Three turbulator configurations were considered, involving one, two, and three identical turbulators, each with a diameter of D = 3 mm and a uniform spacing of SL = 30 mm, positioned at the channel centerline. The governing continuity, momentum, and energy equations were discretized using the finite volume method and solved iteratively using the SIMPLE algorithm. Turbulence effects were modeled using the low-Reynolds-number k–ε turbulence model. The influence of Reynolds number and turbulator count on the friction factor, average Nusselt number, entropy generation, and hydrothermal performance factor was analyzed. Results revealed that increasing the number of turbulators significantly enhances heat transfer and alters flow behavior. Both the average Nusselt number, friction factor, and entropy generation increased with turbulator number. The configuration with three turbulators demonstrated the highest hydrothermal performance, achieving a maximum performance factor of approximately 1.58 at Re = 2000. The numerical results showed good agreement with experimental data, which also employed varying numbers of circular turbulators.

1. Introduction

In recent years, studying the flow Behavior characteristics, heat transfer enhancement, and entropy generation in channels has become very essential due to their importance and many engineering applications. Therefore, turbulators are frequently utilized to enhance thermal performance by fluid mixing and boundary disruption. Numerous turbulator designs have

*Corresponding author: Albashir A. Obeid; alb22e2002@uoanbar.edu.iq; +9647817263024

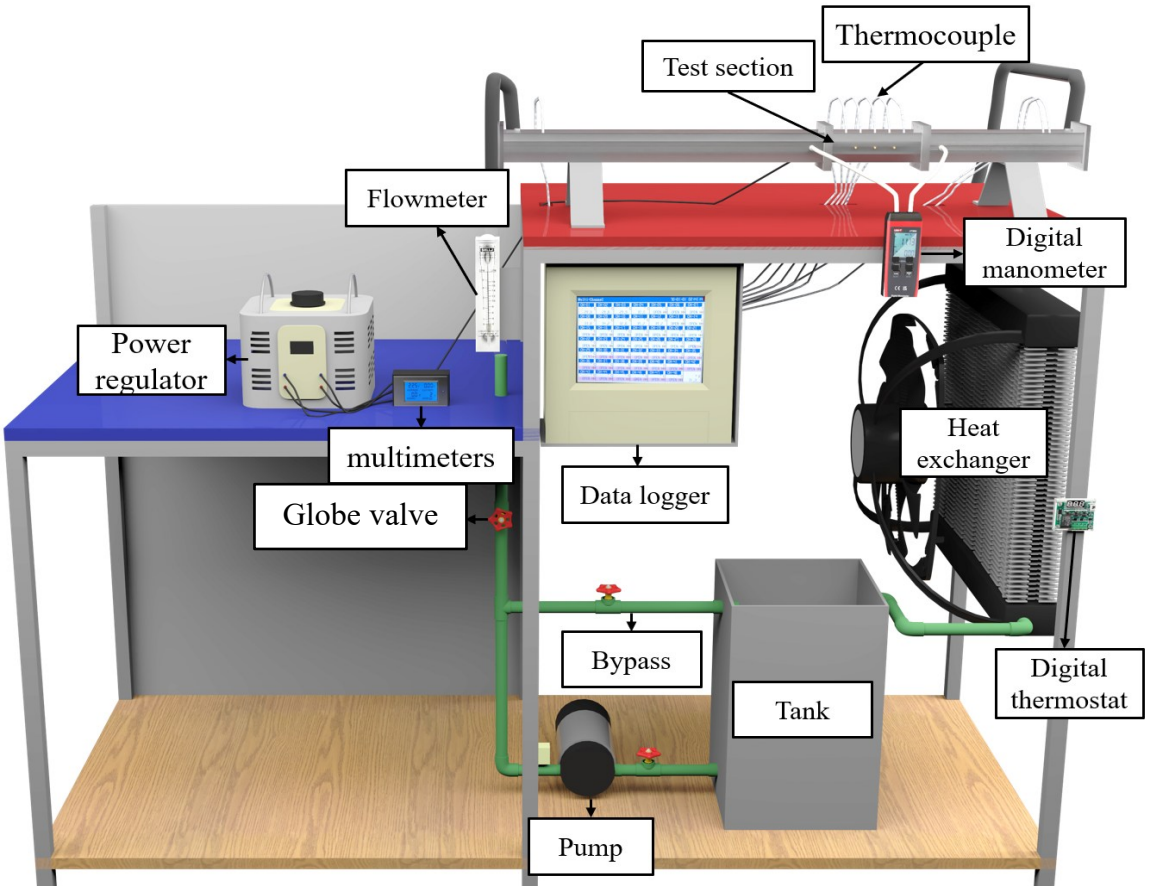

Fig. 1 Experimental schematic diagram of the current study.

been created in recent decades and seek to increase the heat transfer area or coefficient. By disturbing the flow field and inducing localized turbulence, these turbulator inserts break up the thermal boundary layer and enhance convective heat transfer. Several investigators have used both computational and experimental methods to study the flow and heat transfer of a typical fluid with turbulators in the channel. Taslim and Spring [1] experimentally investigated the influence of turbulator configurations on heat transmission in rectangular cooling channels. A turbulator with a height-to-width ratio greater than one improved heat transmission but resulted in increased pressure losses, according to the results. With trapezoidal-shaped turbulators, minimal friction loss and high thermal performance were achieved. When corner rounding was increased or the height-to-width ratio was reduced, the Nusselt number decreased. Pitchandi and Natarajan [2] conducted a theoretical study on entropy generation in circular and elliptical pin fins under forced convection with air, showing that elliptical fins had lower entropy generation at Re < 100. In contrast, circular fins performed better at higher Re, with the optimum slenderness ratio decreasing as the Re increased. Armellini et al. [3] experimentally investigated flow structures in a rectangular cooling channel with a confined circular cylinder at Reynolds numbers of 800, 1800, and 2800. High free-stream turbulence caused early shear layer instabilities and strong vortices, even at low Reynolds numbers. Irregular vortex shedding and complex spanwise wake flows were observed. Eiamsa-ard and Promvonge [4] experimentally studied turbulent airflow in a tube with tandem diamond-shaped turbulators at Reynolds numbers from 3,500 to 16,500. Heat transmission increased with Reynolds number and was highest at a 45° cone angle. Longer tail lengths reduced both heat transmission and friction, while larger cone angles increased friction losses. Alawadhi [5] numerically analyzed laminar forced convection over an in-line array of elliptical cylinders with increasing inclination angles (0° to 90°) at Re from 125 to 1000. Heat transmission improved with higher Re and cylinder inclination, peaking at a 238.59% increase for the fourth cylinder, but causing up to 700% higher pressure

drop. Cheraghi et al. [6] Heat transport in an identically heated mini-channel using a circular cylinder turbulator at a one-third blockage ratio and a Reynolds number of 100 was investigated numerically. Center placement enhanced vortex shedding, boosting mixing and heat transmission. Near-wall placement suppressed shedding, resulting in steady flow, lower heat transmission, and reduced pressure drops. Wang and Zhao [7] numerically analyzed Heat transmission and flow through a rectangular channel using a small circular cylinder to create a vortex generator at a Reynolds number of 3745. Varying the gap ratio from 0 to 6, Results indicated that a gap ratio of 2 optimized heat transmission with an 18.76% Nusselt number increase, while a gap ratio of 0 reduced friction by 13.04%. Zhang et al. [8] numerically studied forced convection over two tandem square cylinders with varying corner radii (0 to 0.5) and gap ratios (1–8) at a Reynolds number of 100. Square-like cylinders produced unsteady wakes, enhancing heat transmission, especially at larger gaps. Rounded corners stabilized flow, reducing heat transmission and drag, with circular cylinders showing the lowest drag. Nilpueng et al. [9] experimentally analyzed the thermal efficiency of square, circular, and shifting square pin fins at Re ranging from 1,700 to 5,200. Square pin fins showed a 12.5% increase in heat transmission coefficients and 15% higher pressure drops compared to circular fins. Rotated square fins further increased heat transfer by 13.1% but caused a 54.8% rise in pressure loss. Furthermore, Bhandari et al. [10] numerically compared heat transmission and friction behavior of nine pin-fin shapes, in a wide rectangular channel for Re from 10,000 to 60,000. The diamond fins exhibited the highest Nusselt numbers and thermal performance, outperforming circular fins by 20% in thermal performance, but faced 60% higher friction factors. Vyas et al. [11] Three distinct blockage numbers, 0.25, 0.38, and 0.5, were investigated experimentally and numerically to determine their effects on influenced heat transmission as well as flow dynamics in a channel using a circular adiabatic cylinder. The results demonstrated that vortex shedding frequency increased by 49%, 98%, and 166% as a percentage for blockage values of 0.5, 0.38, and 0.25, respectively. A blockage ratio of 0.25 yielded the highest average heat transmission coefficient, while a blockage ratio of 0.38 showed the longest downstream influence of vortices. Stąsiek et al. [12] experimentally and numerically analyzed heat transmission and fluid behavior in channels equipped with rib turbulators, and airflow experiments were conducted for Re up to 150,000. Furthermore, Results demonstrated that rib turbulators significantly enhanced local heat transmission, with up to a threefold increase in Nusselt numbers compared to smooth channels. The configuration with ribs on both top and bottom walls yielded a 19% higher Nusselt number near the wall zones due to increased turbulence. Brodnianská and Koťsmíd [13] employed both computational and experimental studies to enhance heat transport in a wavy channel utilizing cylindrical vortex generators with Re ranging from 778 to 7930. According to the findings, the mean Nusselt number of the wavy channel was 1.98 times higher than that of the smooth channels. The Nusselt number in the wavy channel with cylindrical vortex generators increased 3.18 times more than that in the wavy channel without vortex generators, and 6.28 times more than in the smooth channel. Fang et al. [14] numerically investigated the thermal and hydraulic performance of a tube equipped with semi-circular and teardrop-shaped turbulators under constant wall temperature conditions. Eight turbulator configurations were assessed for heat transmission enhancement and pressure drop. Results showed that both turbulator types significantly increased heat transmission, up to 257% for semi-circular and 298% for teardrop-shaped turbulators, compared to a plain tube. However, pressure drops also increased. The teardrop-shaped turbulator demonstrated the highest thermal enhancement factor of 1.27. In another study, Numerical investigation of semi-elliptical protrusions in rectangular microchannels (Re = 1214–8128), and noted that a performance evaluation criterion of 1.80 at Re = 2004. Protrusions increase Nusselt numbers by up to 50% compared to smooth channels at moderate Re due to improved flow mixing from induced turbulence. Friction factors rise to 1.8 times those of smooth channels at high Re. Heat transfer is enhanced by turbulence near the walls, with turbulence zones expanding as Re increases, as studied by H. Sun et al. [15]. Alizadeh et al. [16] numerical investigation of the impact of turbulator geometry on heat transmission enhancement within a square-section channel. Five distinct turbulator geometries were analyzed: semi-cylindrical turbulator (SCT), semi-triangular turbulator (TRT), sharp-point (or sword-type) turbulator (SHT), semi-crescent turbulator (SLT), and rectangular turbulator (RET). The SCT and SLT

geometries exhibited the highest Nusselt numbers and the most significant reduction in friction Coefficients across the tested Reynolds number range 10,000 to 30,000. Kim et al. [17] experimentally conducted the photovoltaic–thermal collector that incorporates both rectangular turbulators and longitudinal fins, aiming to simultaneously enhance electrical and thermal efficiencies. The study found that the electrical efficiency of the collector with both rectangular turbulators and longitudinal fins reached 17.06%, surpassing the smooth (16.55%) and only fins (16.80%). In terms of thermal efficiency, turbulators and fins achieved 38.93%, while the smooth and only fins reached 22.68% and 33.56%, respectively. Liao et al. [18] numerically studied the heat transmission enhancement in microchannel systems by combining vortex generator designs with nanofluids. Simulations explored the effects of vortex generator size, shape, and nanoparticle concentration at a moderate flow rate. Results showed that larger vortex generators improved heat transmission but caused significant flow resistance. Rectangular vortex generators with high aspect ratios lowered the pressure drop by over 75 % and slightly improved performance. Adding nanofluids further enhanced heat transmission; at a small concentration of 0.6%, heat transmission increased noticeably with only a minor increase in pressure drop. Xi and Meng [19] numerically studied flow and heat transmission in a rectangular mini-channel with interpolated double S-shaped turbulators using ANSYS Fluent. The study examined the effects of different axial radii (1 mm, 1.5 mm, and 2 mm).At Reynolds numbers from 250 to 2550, the turbulators enhanced heat transmission by up to 101.74% and reduced thermal resistance by 50.72%. The 2 mm radius offered the best thermal efficiency with moderate pressure loss. Mei et al. [20] numerically analyzed the thermal-hydraulic performance of a grooved cone turbulator in a heated tube under turbulent flow (Re = 4,190–25,140). Heat transmission improved with larger groove diameters and twist angles, but decreased with longer pitch. The turbulator boosted the Nusselt number by up to 762%, with a peak thermal enhancement factor of 3.51. Bhandari et al. [21] experimentally evaluated the effect of prism pin sides in a microchannel heat sink, revealing that four-sided prisms perform best, with Nusselt numbers 18% higher than triangular prisms and 7% better than prisms with more sides. Increasing sides beyond five has a negligible impact. In other studies focused on entropy generation, Karakus et al. [22] experimentally analyzed heat transmission and entropy generation in a circular pipe with one to three spherical turbulators under turbulent flow using water. Results showed that three turbulators increased the Nusselt number by over 80%, tripled the friction factor, achieved a performance factor of 1.28, and reduced total entropy generation due to lower thermal irreversibility. Bayat et al. [23] numerically evaluated the effects of a cam vortex generator on heat transmission and entropy generation in a microchannel at Re from 100 to 800. Results showed increased attack angle, enhancing thermal uniformity but raising viscosity, friction losses, and reducing entropy generation.

In light of these reviewed studies, it is clear that many previous investigations have explored turbulators of various shapes for improving heat transfer performance in channel flows. However, there is still a lack of systematic analysis addressing adiabatic turbulators under turbulent conditions, particularly focusing on their entropy generation characteristics and performance evaluation criteria across a range of geometrical configurations. Moreover, the role of adiabatic circular turbulators in decoupling pure flow-induced enhancements from thermal experimental and numerical conduction effects has not been thoroughly examined. Therefore, this study aims to fill these research gaps by experimentally and numerically investigating the hydrothermal and entropy generation performance of adiabatic circular turbulators with different counts. The originality of this work lies in providing new quantitative insights into the secondary flow mechanisms, entropy distribution, and performance trade-offs associated with circular turbulence promoters. These insights are relevant for designing compact, energy-efficient cooling devices in applications such as electronic thermal management, automotive heat exchangers, and advanced energy systems.

2. Experimental procedure

2.1. Experimental setup

The experimental schematic diagram for the current study is in Fig. 1. The essential components of the experimental setup are an Electrical heater, an AC power regulator, type-K thermocouples, a digital multimeter, a digital manometer, a thermostat, a water loop, a test section, and a digital data logger.

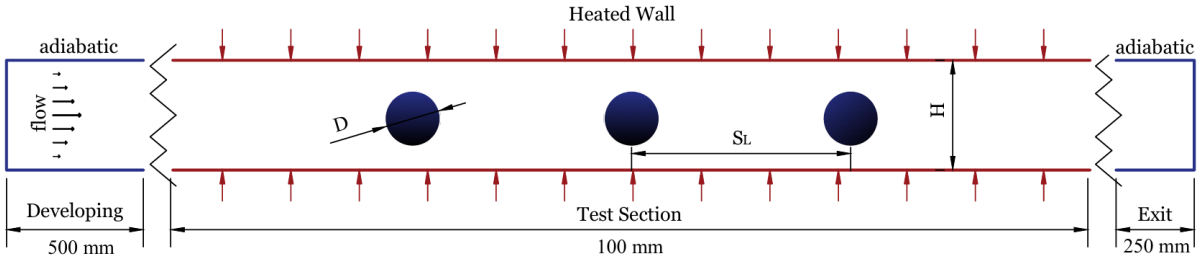

Fig. 2 Geometry of the current study.

A 0.15-horsepower pump was used to pump the working fluid through the test section. The upper and lower walls of the test section were heated using two electric heater plates, each with a maximum power output of 320 W. These heaters were mounted on the back surfaces of the top and bottom walls of the test section. To minimize heat loss to the surroundings, the test section was insulated with two layers of glass wool, each 10 cm thick, and with an approximate density of 32 kg/m^3.

An AC power regulator was used to control the voltage and current supplied to the heaters, and a digital multimeter was connected to the circuit to verify the input parameters. Wall and fluid temperatures were measured using K-type thermocouple probes connected to a KH448G-U-NN data logger to show the temperature value on the screen. To measure the wall temperature distribution, five thermocouple probes were embedded in the rear side of the upper wall of the test section. These were inserted into 2 mm diameter holes drilled at distances of 17, 37, 57, 77, and 97 mm from the test section inlet and sealed with thermal epoxy.

For fluid temperature measurement, two thermocouple probes were placed at the inlet, and two additional ones were positioned within the outlet to measure the bulk fluid temperature. All thermocouples were pre-calibrated at different temperatures to ensure accuracy with an uncertainty of ±1%. The flow rate was measured using an LZM-15T flow meter, installed between the pump and the developing section's inlet. This device measures flow rates between 2 and 18 LPM with an accuracy of ±5.0%. As a secondary calibration check, the bucket-and-stopwatch method was employed. The pump flow rate was adjusted using a bypass line equipped with a globe valve for precise flow control and preventing the flow from putting pressure on the pump. During experiments, distilled water was used as the working fluid, and its temperature was maintained at 27 °C.

A digital manometer (UT366A) was connected to pressure taps at the inlet and outlet of the test section to measure the differential pressure with an accuracy of ±0.5%. During testing, key parameters such as pressure drop, flow rate, bulk fluid temperature (at inlet and outlet), and wall temperature were recorded once steady-state conditions were achieved. This procedure was repeated for various flow rates and different configurations of circular turbulators. Subsequent to the discussion of the setup, the test section is introduced, as it forms the central part of the apparatus where the experimental investigations were performed.

2.2. Test section

It consists of two side walls and the top and bottom (main) walls. The test portion's upper and bottom walls were constructed from aluminum plates that measured 100 mm in length, 55 mm in width, and 4 mm in thickness. An acrylic that was 6 mm thick was used for the test section side walls in order to minimize heat loss to the surroundings. Two axial grooves are positioned along the side wall of each of them to prevent fluid from leaking out of the test area. Thermal epoxy was used to seal the side walls and construct the test section. As seen in Fig. 2, three distinct numbers of straight and circular turbulator channels were constructed and tested for this investigation. However, the circular turbulator, D, had a diameter of 3 mm, and the distance between turbulators, SL, was 30 mm; These parameters were selected to provide a balance between heat transfer enhancement and frictional losses, consistent with values reported in several previous studies, such as [11]. Two adiabatic straight sections were used to create appropriate conditions for the test section's inflow and outflow: a 500 mm long acrylic duct upstream and a 250 mm long acrylic duct downstream. the discussion of the practical components, the

analytical framework is introduced, including the governing equations and data reduction procedures employed to calculate the main performance parameters such as Reynolds number, Nusselt number, and friction factor.

2.3. Data reduction

The following is the expression for the heat that the working fluid acquired from the test section [24]:

$$Q_f = \dot{m}_f C_{p,f} (T_{b,o} - T_{b,in}) \quad (1)$$

The following is the average heat transfer coefficient. [24]:

$$h_{avg} = \frac{Q_f}{A_s (T_{w,avg} - T_{b,avg})} \quad (2)$$

The following formula could be use to calculate average Nusselt number [24]:

$$Nu_{avg} = \frac{h_{avg} D_h}{k_f} \quad (3)$$

D_h is the channel's hydraulic diameter, which is defined as:

$$D_h = \frac{4A}{P} \quad (4)$$

The performance evaluation criteria (PEC) can be defined as [25]:

$$PEC = \frac{(Nu/Nu_s)}{(f/f_s)^{1/3}} \quad (5)$$

Where f is the factor of friction, evaluated as [26]:

$$f = \Delta p \frac{D_h}{L} \frac{2}{\rho_f u_{in}^2} \quad (6)$$

In the equation above, Δp is the pressure drop which is evaluated as follows:

$$\Delta p = p_{in} - p_{out} \quad (7)$$

Total entropy generation is defined as follows[27]:

$$sg = \frac{q^2}{4T_{avg}^2 \dot{m} C_p} \frac{D\,Re}{Nu\,Pr} + \frac{2\dot{m}^3}{\rho^2 T_{avg}} \frac{f}{DA_C^2} \quad (8)$$

The heat gained by the fluid, calculated from Eq. (1), was 44.1 W. Using Eq. (2), the convective heat-transfer coefficient was h=1597.2 W/k.m^2. Consequently, the average Nusselt number was Nu=36.96 at Re=2000.

2.4. Uncertainty analysis

The Kline and McClintock [28] method was used to compute the experimental uncertainties of the dependent parameters in this investigation, including the Re, f, and Nu. For example, given the key parameters, R, as follows:

$$R = R(X_1, X_2, X_3, \ldots\ldots, X_n) \quad (9)$$

The independent measured parameters in this case are X_1, X_2, X_3 and X_n . Therefore, the following is the method by which the uncertainty of R is calculated:

$$U_R = \pm \sqrt{\left(\frac{\partial R}{\partial X_1} U_{X_1}\right)^2 + \left(\frac{\partial R}{\partial X_2} U_{X_2}\right)^2 + .. + \left(\frac{\partial R}{\partial X_n} U_{X_n}\right)^2} \quad (10)$$

As a result, the Nu, Re, and f were all within 9.8751% ±, 5.3059% ±, and 10.4482% ±, respectively.

3. Mathematical formulation

3.1. Problem Description

The geometry of the current study is shown in Figure 2. It consists of three identical adiabatic turbulators, with a spacing of 30 mm, and has been located at the center of the channel. The diameter of the turbulator considered in this study is 3 mm. The selection of geometric parameters was guided by previous studies that demonstrated significant thermal enhancement with similar blockage ratios. The chosen values offer a balance between enhancing flow disturbance and minimizing excessive pressure drop. To ensure fully developed flow conditions, two adiabatic straight sections were used upstream and downstream of the heated region. The upstream adiabatic section measured 500 mm in length, and the downstream section measured 250 mm. These regions were thermally insulated to prevent heat exchange with the surroundings. Distilled water was used as the working fluid throughout the setup. The flow was assumed to be turbulent, steady, and incompressible. The channel's width significantly exceeded its height, allowing the geometry to be approximated as two-dimensional, with no-slip boundary conditions applied to the walls, and the buoyancy forces were neglected. The test section wall was subjected to a constant heat flux of q = 5 kW/m^2. To enhance computational efficiency and reduce processing time, only the upper half of the channel was considered in the numerical solution, with a symmetry boundary condition applied at the

channel's centreline. This subsection introduces the physical model and geometrical configuration of the present study. The problem description defines the channel dimensions, turbulator arrangement, and boundary assumptions, which establish the foundation for both the numerical analysis and experimental validation.

3.2. Governing Equations

The following is an expression for the two-dimensional Continuity, momentum, and Energy governing equations in Cartesian coordinates [29]:

Continuity equation:

$$\frac{\partial}{\partial x}(\rho u)+\frac{\partial}{\partial y}(\rho v)=0 \tag{11}$$

U-momentum equation:

$$\frac{\partial}{\partial x}(\rho uu)+\frac{\partial}{\partial y}(\rho uv)=-\frac{\partial p}{\partial x}+\frac{\partial}{\partial x}\left(\mu_e\frac{\partial u}{\partial x}\right)+\frac{\partial}{\partial y}\left(\mu_e\frac{\partial u}{\partial y}\right)+\frac{\partial}{\partial x}\left(\mu_e\frac{\partial u}{\partial x}-\frac{2}{3}\rho k\right)+\frac{\partial}{\partial y}\left(\mu_e\frac{\partial v}{\partial x}\right) \tag{12}$$

V-momentum equation:

$$\frac{\partial}{\partial x}(\rho uv)+\frac{\partial}{\partial y}(\rho vv)=-\frac{\partial p}{\partial y}+\frac{\partial}{\partial x}\left(\mu_e\frac{\partial v}{\partial x}\right)+\frac{\partial}{\partial y}\left(\mu_e\frac{\partial v}{\partial y}\right)+\frac{\partial}{\partial x}\left(\mu_e\frac{\partial u}{\partial y}\right)+\frac{\partial}{\partial y}\left(\mu_e\frac{\partial v}{\partial y}-\frac{2}{3}\rho k\right) \tag{13}$$

where, $\mu_e=\mu+\mu_t$

Energy equation:

$$\frac{\partial}{\partial x}(\rho uT)+\frac{\partial}{\partial y}(\rho vT)=\frac{\partial}{\partial x}\left(\Gamma_T\frac{\partial T}{\partial x}\right)+\frac{\partial}{\partial y}\left(\Gamma_T\frac{\partial T}{\partial y}\right) \tag{14}$$

$$where, \Gamma_T=\frac{\mu}{Pr}+\frac{\mu_t}{Pr_t}$$

Typically, the k-ε turbulence model, which is widely used, includes two equations designed to determine the turbulent dynamic viscosity μt, which is determined by the dissipation rate ε and the turbulent kinetic energy k. One of the most often used turbulence models is the k-ε model, which was proposed by Launder and Sharma [30] . The low-Reynolds-number form of the k–ε turbulence model was selected in this study due to its capability to resolve the near-wall regions without the need for wall functions. This approach ensures accurate representation of viscous sublayers and is suitable for the Reynolds number range investigated.

Turbulent kinetic Energy equation[30]:

$$\frac{\partial}{\partial x}(\rho uk)+\frac{\partial}{\partial x}(\rho vk)=\frac{\partial}{\partial x}\left(\Gamma_k\frac{\partial k}{\partial x}\right)+\frac{\partial}{\partial y}\left(\Gamma_k\frac{\partial k}{\partial y}\right)+P_k-\rho(\varepsilon+\varepsilon_w) \tag{15}$$

$$where, \Gamma_k=\mu+\frac{\mu_t}{\sigma_k}$$

Production rate[30]:

$$P_k=\mu_t\left\{2\left[\left(\frac{\partial u}{\partial y}\right)^2+\left(\frac{\partial v}{\partial x}\right)^2\right]+\left(\frac{\partial u}{\partial y}+\frac{\partial v}{\partial x}\right)^2-\frac{2}{3}\rho k\left(\frac{\partial u}{\partial x}+\frac{\partial v}{\partial y}\right)\right\} \tag{16}$$

Dissipation rate at wall[30]:

$$\varepsilon_w=2\frac{\mu}{\rho}\left[\left(\frac{\partial\sqrt{k}}{\partial x}\right)^2+\left(\frac{\partial\sqrt{k}}{\partial y}\right)^2\right] \tag{17}$$

Turbulent kinetic energy dissipation equation:

$$\frac{\partial}{\partial x}(\rho u\varepsilon)+\frac{\partial}{\partial y}(\rho v\varepsilon)=\frac{\partial}{\partial x}\left(\Gamma_\varepsilon\frac{\partial\varepsilon}{\partial x}\right)+\frac{\partial}{\partial y}\left(\frac{\partial\varepsilon}{\partial y}\right)+\left(C_1f_1P_k-C_2f_2\varepsilon\right)\frac{\varepsilon}{k}+\varphi_\varepsilon \tag{18}$$

$$where, \Gamma_k=\mu+\frac{\mu_t}{\sigma_\varepsilon}$$

$$\varphi_\varepsilon=2\mu_t\frac{\mu}{\rho}\left[\left[\left(\frac{\partial^2u}{\partial x^2}\right)^2+\left(\frac{\partial^2v}{\partial x^2}\right)^2\right]+2\left(\frac{\partial^2u}{\partial x\partial y}\right)^2+2\left(\frac{\partial^2v}{\partial x\partial y}\right)^2+\left(\frac{\partial^2v}{\partial y^2}\right)^2\right] \tag{19}$$

The turbulent eddy viscosity:

$$\mu_t=C_\mu f_\mu\rho\left(\frac{k^2}{\varepsilon}\right) \tag{20}$$

Empirical constants & turbulent Prandtl number[30]:

$$C_\mu=0.09,\ C_1=1.44,\ C_2=1.92, \tag{21}$$

$$\sigma_k=1.0,\ \sigma_\varepsilon=1.3,\ Pr_t=0.9 \tag{22}$$

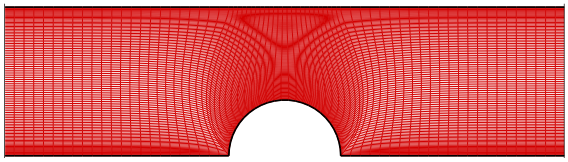

Fig. 3 The computational mesh for this work.

Wall damping functions[30]:

$$f_1=1.0,\ f_2=1\text{-}0.3\exp\left(\text{-}Re_T^2\right) \quad (23)$$

$$f_\mu=exp\left[\frac{\text{-}3.4}{(1+0.02Re_T)^2}\right] \quad (24)$$

Turbulent Reynolds number[30]:

$$Re_T=\frac{\rho}{\varepsilon}\left(\frac{k^2}{\mu}\right) \quad (25)$$

Thermal entropy generation [31]:

$$s_{g,th}=\frac{k_f}{T^2}\left[\left(\frac{\partial T}{\partial x}\right)^2+\left(\frac{\partial T}{\partial y}\right)^2\right] \quad (26)$$

Viscous entropy generation [31]:

$$s_{g,v}=\frac{\mu_f}{T}\left\{\left[2\left(\frac{\partial u}{\partial x}\right)^2+\left(\frac{\partial v}{\partial y}\right)^2\right]+\left(\frac{\partial u}{\partial y}\right)^2+\left(\frac{\partial v}{\partial x}\right)^2\right\} \quad (27)$$

The overall entropy generation is formally defined as follows: [31]:

$$s_g=s_{g,th}+s_{g,v} \quad (28)$$

3.3. Boundary conditions

Appropriate boundary conditions for each dependent variable must be specified for all. Computational domain boundaries to solve the governing equations. The following is how these boundary conditions are presented:

- Inlet Boundary

$$u=u_{in}=\frac{\mu_f Re}{\rho_f D_h},\ v=0\ ,\ T_{in}=298\ K \quad (29)$$

$$K=K_{in}=\frac{2}{3}(I_o\,u_{in})^2 \quad (30)$$

$$\varepsilon=\varepsilon_{in}=\frac{C_\mu^{3/4}\,K_{in}^{3/2}}{0.07\,D_h} \quad (31)$$

In the current study, the turbulence intensity value (I_o) at the inlet of the channel region is 0.05 [24].

- Outlet boundary

$$\frac{\partial u}{\partial x}=0,\ \frac{\partial v}{\partial x}=0,\ \frac{\partial T}{\partial x}=0,\ \frac{\partial K}{\partial x}=0,\ \frac{\partial \varepsilon}{\partial x}=0. \quad (32)$$

- Wall Boundary

$$u=0,\ v=0,\ k=0,\ \varepsilon=0. \quad (33)$$

$\frac{\partial T}{\partial \eta}$ *= 0 (along the turbulator, developing, and exit section walls)*

$\frac{\partial T}{\partial \eta}=\frac{q_w}{k_f}$ *(along the walls of test section)*

- Symmetry line Boundary

$$\frac{\partial u}{\partial y}=0,\ \frac{\partial v}{\partial y}=0,\ \frac{\partial T}{\partial y}=0,\ \frac{\partial K}{\partial y}=0,\ \frac{\partial \varepsilon}{\partial y}=0. \quad (34)$$

To ensure a well-posed numerical problem, appropriate boundary conditions are specified for all dependent variables. These conditions define the flow, thermal, and turbulence characteristics at the inlet, outlet, walls, and symmetry plane of the computational domain."

3.4. Numerical solution

In this work, a FORTRAN code was developed to solve the governing equations of continuity, momentum, energy, and turbulence. The finite volume technique (FVM) is used to discretize the governing equations. The central differencing scheme is used to discretize the diffusion term and the upwind term for the convection in the governing equations. The pressure field was calculated by connecting the velocity and pressure equations using the SIMPLE algorithm. In the current investigation, all dependent variables are stored at the same control volume using a collocated grid layout. As a result, the pressure and velocity components have a weak relationship. In order to prevent the unreal pressure oscillation, a pressure nodes was established using the Rhie and Chow momentum interpolation method. Additionally, the computational mesh for this work is developed using Poisson equations, as shown in Figure 3. A better convergence behavior is obtained by applying under-relaxation. When the total absolute residual for all variables over the computational domaindirect connection between

the velocity and the is less than $1x10^{-5}$, the computation is completed.

Although the study provides valuable insight into the thermal and entropy behavior of turbulator-equipped channels, several limitations should be acknowledged. First, while the low-Re k–ε turbulence model was suitable for the studied Reynolds number range, other models may yield different quantitative predictions, though the

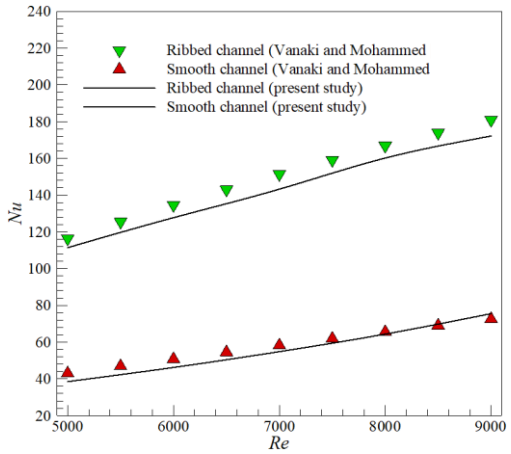

Fig. 4 Average Nusselt number for the present investigation compared to the numerical investigation of Vanaki and Mohammed [31].

overall performance trends are expected to remain similar. Second, the conclusions are valid for steady, incompressible, single-phase flow under constant heat flux; different flow regimes or

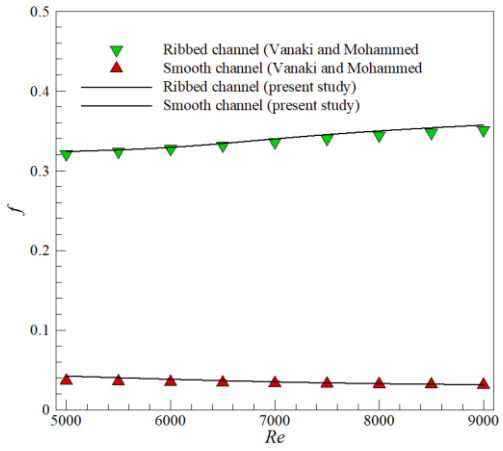

Fig. 5 Friction factor for the present investigation compared to the numerical investigation of Vanaki and Mohammed [31].

thermal boundary conditions could alter the results. Finally, the analysis was limited to distilled water as the working fluid. Although the methodology can be applied to other fluids, variations in viscosity, thermal conductivity, or heat capacity would influence the outcomes.

4. Validation of numerical methods and grid independence test

The accuracy of the CFD code developed for the present investigation has generally been verified through a number of comparisons with previous investigations. This section presents the comparison between the current study and the numerical analysis of Vanaki and Mohammed [31]. In their investigation, the ribbed channel height was 10 mm and the total length of the channel was 340 mm. It is assumed that the top and bottom walls of the channel were maintained at a uniform heat flux of 10 kW/m^2. Figures 4 and 5 demonstrate how the current results compare to the Nu and f of a two-dimensional confined ribbed channel and smooth for a previous numerical study. It was seen that good results were attained. Additionally, there was a deviation for the ribbed channel of 12.51% and 5.80% for the Nu and the f, respectively. Also, the deviation for the smooth channel was 7.34% and 2.79% for the Nu and the f, respectively.

The precision of the numerical results is often determined by the grid resolution. For this investigation, five different mesh sizes have been used in order to verify mesh independence. Using circular turbulators. It was discovered that grid independence results may be obtained with a mesh size of 851x101, which consists of 851 grid nodes in the X axis and 101 grid nodes in the Y axis.

Table 1: GIT of three turbulators with Re = 5000.

Grid Size	Nu	f	Deviation (%)	
			Nu	f
551×71	61.28174	0.67327	8.14	7.41
651×81	58.91865	0.64706	3.97	3.23
751×91	57.38292	0.63359	1.26	1.08
851×101	56.85082	0.62852	0.32	0.27
951×111	56.66889	0.62682	Baseline data	

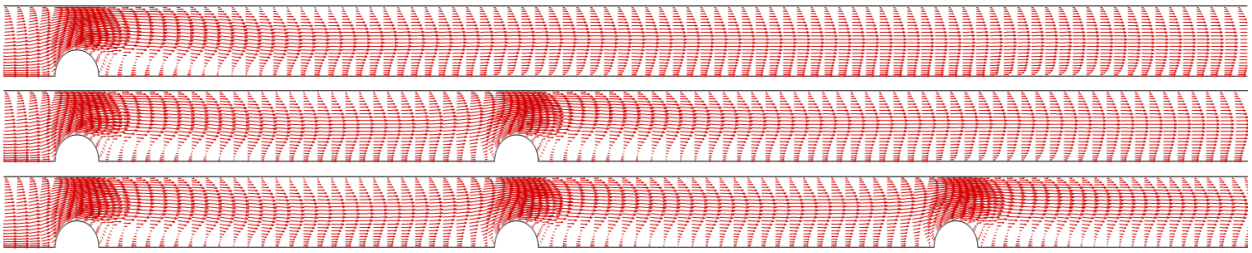

Fig. 6 Velocity vector for different circular turbulator numbers at Re = 5000.

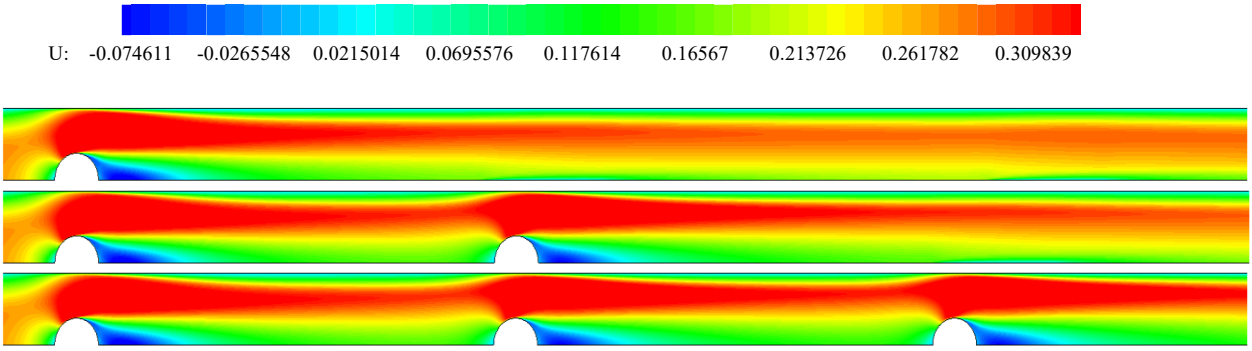

Fig. 7 Velocity contours for different circular turbulator numbers at Re = 5000.

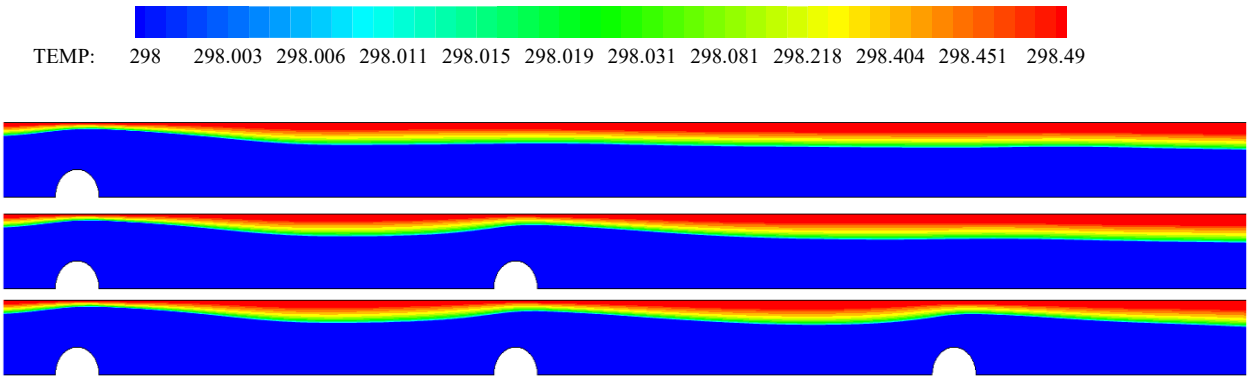

Fig. 8 Temperature contours for different circular turbulator numbers at Re = 5000.

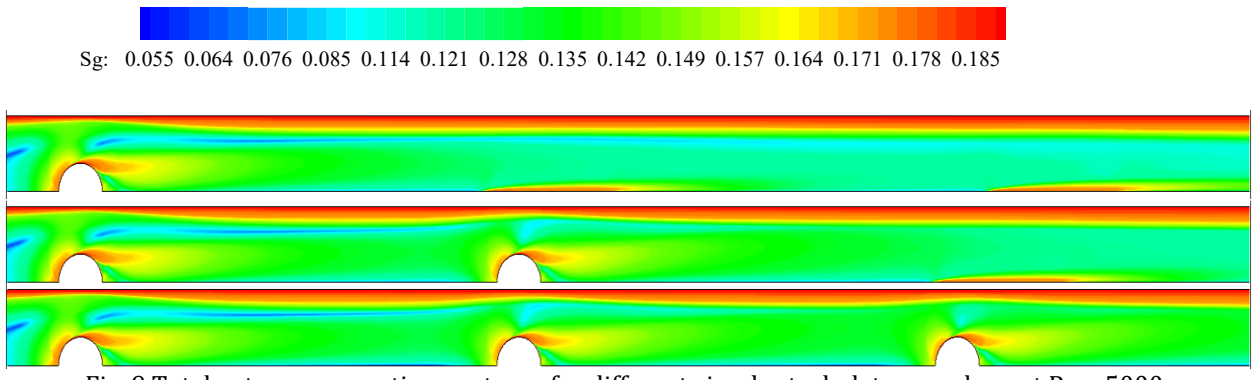

Fig. 9 Total entropy generation contours for different circular turbulator numbers at Re = 5000.

5. Results and discussions

Figures 6 and 7 depict the velocity vectors and streamwise velocity contours from the numerical simulations at Re = 5000 for various turbulator configurations. The results clearly show that both Reynolds number and turbulator count strongly influence the flow dynamics. As Re increases, inertial forces dominate over viscous effects, resulting in the formation of larger and more energetic recirculation zones downstream of each turbulator. These vortices enhance transverse mixing by promoting strong interaction between the near-wall flow and the channel core. Moreover, increasing the number of turbulators intensifies flow obstruction, leading to more frequent flow separation and vortex shedding. This mechanism increases turbulence intensity and enhances secondary flows, especially in the 3T case, where overlapping wake structures amplify local velocity gradients and mixing efficiency.

Figure 8 presents the corresponding temperature contours at Re = 5000. The thermal boundary layer is directly above the turbulators due to localized

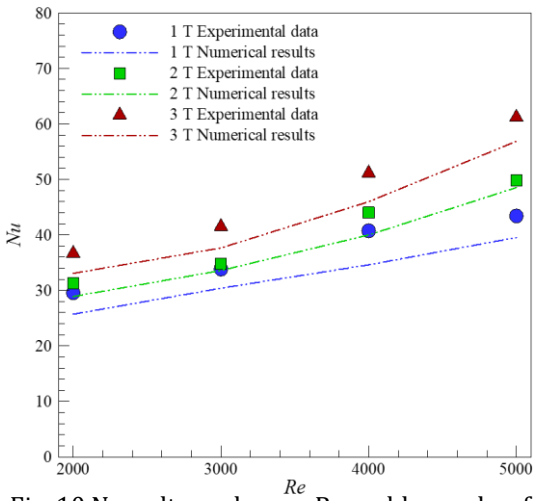

Fig. 10 Nusselt number vs. Reynolds number for different numbers of circular turbulators.

acceleration and flow impingement. As the number of turbulators increases, these effects become more pronounced, producing steeper wall-normal temperature gradients. This disruption of thermal stratification facilitates continuous renewal of the heated fluid layer, thereby increasing convective heat transfer. The enhanced fluid mixing induced by strong recirculation improves thermal homogeneity and promotes better heat extraction from the wall.

Figure 9 shows the total entropy generation contours, incorporating both viscous and thermal contributions. Entropy generation peaks at regions of high shear (around the turbulators) and steep thermal gradients (along heated walls). The total entropy increases with the number of turbulators due to more intense flow disturbances and frictional dissipation. Although heat transfer is improved, the accompanying rise in pressure losses and thermal irreversibilities reflects a trade-off between thermal performance and thermodynamic efficiency.

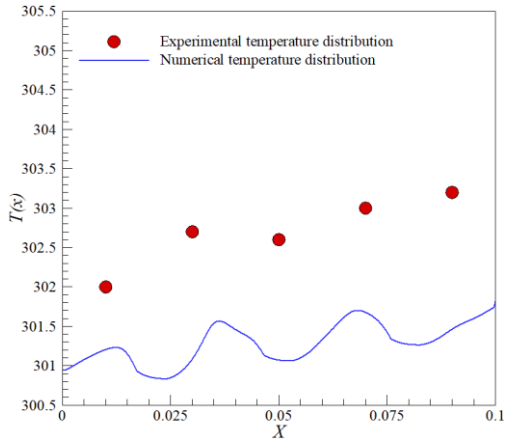

Fig. 11 Experimental and Numerical wall temperature distribution across the channel.

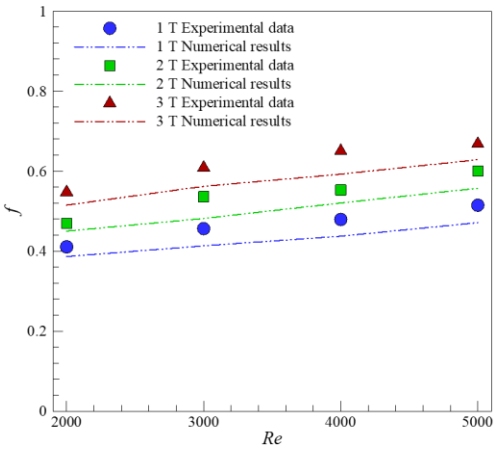

Fig. 12 Friction factor vs. Reynolds number for different numbers of circular turbulators.

Figure 10 illustrates that the average Nusselt number increases with both the Reynolds number and the number of turbulators. Also, Figure 11 show the experimental and numerical wall temperature distribution across the channel. This

trend is attributed to the thinning of the thermal boundary layer caused by stronger inertial forces at higher Re, as well as intensified secondary flows and vortex interactions with increasing turbulator count. These effects enhance wall-normal temperature gradients and promote better thermal mixing, leading to higher convective heat transfer rates. Among the tested configurations, 3T exhibited the highest Nu values due to the synergy between enhanced turbulence and effective disruption of thermal stratification. The numerical

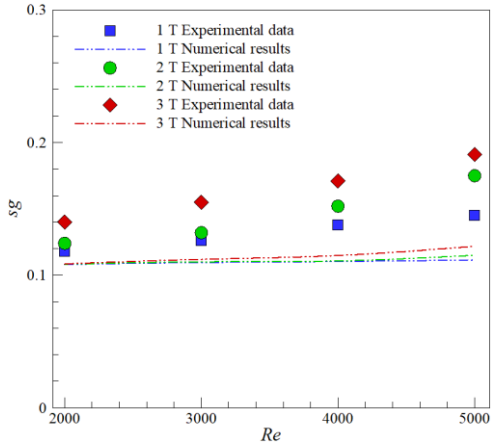

Fig. 13 Total entropy generation vs. Reynolds number for different numbers of circular turbulators.

results show good agreement with experiments, with an average deviation of 9.11%.

Figure 12 compares the friction factor obtained from both experimental and numerical results. It is evident that the friction factor increases with both the Reynolds number and the number of turbulators. The rise with Re is attributed to steeper velocity gradients near the walls at higher flow speeds, which elevate wall shear stress. Adding turbulators intensifies this effect by inducing flow separation and recirculatory wakes, thereby increasing turbulence intensity and form drag. Configurations with more turbulators, such as 3T, generate stronger vortex shedding and larger wake zones, resulting in greater viscous and pressure losses. The numerical and experimental results show reasonable agreement, with an average deviation of approximately 13.43%.

Figure 13 illustrates the effect of turbulator number on total entropy generation for various Reynolds numbers. Both experimental and numerical results show a consistent increase in entropy generation with rising Re and turbulator count. Theoretically, this is attributed to intensified velocity and temperature gradients, which drive viscous and thermal dissipation—the two fundamental sources of entropy in convective systems. Practically, the presence of more turbulators extends regions of high shear and thermal non-uniformity, especially downstream of the elements, leading to higher irreversible losses. Although these configurations enhance heat transfer, the increased frictional and conductive effects render them thermodynamically less efficient in terms of entropy generation. The figure shows that there is a high percentage of deviation between the experimental and numerical results, but this is because the results depend on friction and the heat transfer, which already have a percentage of difference or deviation.

Figure 14 presents the performance evaluation criteria (PEC) as a function of Reynolds number and turbulator count, based on both numerical and experimental results. The PEC increases with the number of turbulators, reaching its peak for the 3T

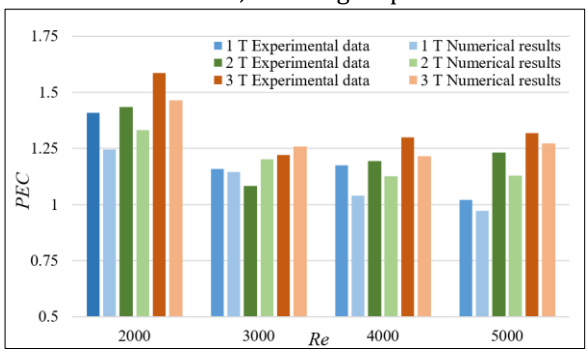

Fig. 14 Performance evaluation criteria vs. Reynolds number for different numbers of circular turbulators.

configuration, particularly at Re = 2000. This trend reflects the balance between enhanced heat transfer and the associated pressure drop. Theoretically, PEC improves when the relative gain in convective heat transfer outweighs the increase in flow resistance. Experimentally, the 3T case exhibited the highest Nu and PEC despite its higher friction and entropy losses, confirming that the thermal benefit dominates. The average deviation between simulation and experiment was 10.98%, validating the consistency between both approaches.

6. Conclusion

This study aimed to investigate the effect of circular adiabatic turbulators on the hydrothermal and

thermodynamic performance of turbulent forced convection in a heated channel, within a Reynolds number range of 2000–5000. Both experimental and numerical approaches were applied, with a FORTRAN-based finite volume solver used to model continuity, momentum, energy, and turbulence equations. The SIMPLE algorithm with Rhie–Chow interpolation, Poisson-based mesh generation, and under-relaxation techniques ensured numerical stability and convergence.

The main findings can be summarized as follows:

- Increasing the number of turbulators enhanced vortex interaction, secondary flows, and reduced the thermal boundary layer thickness, leading to higher heat transfer. However, this improvement was accompanied by increased entropy generation and pressure drop due to stronger flow separation and thermal gradients.
- The 3T configuration exhibited superior performance, achieving a maximum Nusselt number of 56.8 and a highest PEC value of 1.54 at Re = 2000.
- Numerical predictions showed good agreement with experimental results, with average deviations of 9.11% for Nu, 13.43% for f, and 10.98% for PEC, confirming the model reliability.
- The 3T configuration provided the most efficient trade-off between heat transfer enhancement and thermodynamic cost, making it a strong candidate for compact and high-performance thermal systems.

Nomenclature

C_p	specific heat, J/Kg k
D	diameter, m
D_h	hydraulic diameter, m
f	friction factor
H	Channel height
K	thermal conductivity, W/m. ^oC
Nu	Nusselt number, ($Nu=h\ D_h/K_f$)
PEC	Performance Evaluation Criteria
Pr	Prandtl number
q	Heat flux (kW/m^2)
Re	Reynolds number ($Re=\rho_f u_{in} D_h/\mu_f$)
S_L	Space length between turbulators (mm)
T	Temperature
u,v	components of velocities, m/s
x, y	cartesian coordinates, m
k	Turbulent kinetic energy
Greek Symbols	
μ	dynamic viscosity, $N.s/m^2$
ρ	density, kg/m^3
Δp	Pressure drop, pa
ε	Turbulent dissipation rate

Funding

None

References

[1] M. E. Taslim and S. D. Spring, "Effects of turbulator profile and spacing on heat transfer and friction in a channel," *J. Thermophys. Heat Transf.*, vol. 8, no. 3, pp. 555–562, 1994, doi: 10.2514/3.578.

[2] K. Pitchandi and N. E, "Entropy Generation in Pin Fins of Circular and Elliptical Cross-Sections in Forced Convection with Air," *Int. J. Thermodyn.*, vol. 11, Dec. 2008, doi: 10.5541/ijot.224.

[3] A. Armellini, L. Casarsa, and P. Giannattasio, "Separated flow structures around a cylindrical obstacle in a narrow channel," *Exp. Therm. Fluid Sci.*, vol. 33, no. 4, pp. 604–619, 2009, doi: 10.1016/j.expthermflusci.2008.12.005.

[4] S. Eiamsa-ard and P. Promvonge, "Thermal characterization of turbulent tube flows over diamond-shaped elements in tandem," *Int. J. Therm. Sci.*, vol. 49, no. 6, pp. 1051–1062,

2010, doi: 10.1016/j.ijthermalsci.2009.12.003.

[5] E. M. Alawadhi, "Laminar Forced Convection Flow Past an In-Line Elliptical Cylinder Array With Inclination," *J. Heat Transfer*, vol. 132, no. 7, Jul. 2010, doi: 10.1115/1.4000061.

[6] M. Cheraghi, M. Raisee, and M. Moghaddami, "Effect of cylinder proximity to the wall on channel flow heat transfer enhancement," *Comptes Rendus - Mec.*, vol. 342, no. 2, pp. 63–72, 2014, doi: 10.1016/j.crme.2013.12.004.

[7] J. Wang and Y. Zhao, "Heat and fluid flow characteristics of a rectangular channel with a small diameter circular cylinder as vortex generator," *Int. J. Therm. Sci.*, vol. 92, pp. 1–13, Jun. 2015, doi: 10.1016/j.ijthermalsci.2015.01.018.

[8] W. Zhang, X. Chen, H. Yang, H. Liang, and Y. Wei, "Forced convection for flow across two tandem cylinders with rounded corners in a channel," *Int. J. Heat Mass Transf.*, vol. 130, pp. 1053–1069, 2019, doi: 10.1016/j.ijheatmasstransfer.2018.10.125.

[9] K. Nilpueng *et al.*, "Effect of pin fin configuration on thermal performance of plate pin fin heat sinks," *Case Stud. Therm. Eng.*, vol. 27, p. 101269, Oct. 2021, doi: 10.1016/j.csite.2021.101269.

[10] J. Xu, K. Zhang, J. Duan, J. Lei, and J. Wu, "Systematic Comparison on Convective Heat Transfer Characteristics of Several Pin Fins for Turbine Cooling," *Crystals*, vol. 11, no. 8, p. 977, Aug. 2021, doi: 10.3390/cryst11080977.

[11] A. Vyas, B. Mishra, and A. Srivastava, "Investigation of the effect of blockage ratio on flow and heat transfer in the wake region of a cylinder embedded in a channel using whole field dynamic measurements," *Int. J. Therm. Sci.*, vol. 153, no. February, p. 106322, 2020, doi: 10.1016/j.ijthermalsci.2020.106322.

[12] J. Stasiek, A. Stasiek, and M. Szkodo, "Modeling of passive and forced convection heat transfer in channels with rib turbulators," *Energies*, vol. 14, no. 21, 2021, doi: 10.3390/en14217059.

[13] Z. Brodnianská and S. Kotšmíd, "Heat transfer enhancement in the novel wavy shaped heat exchanger channel with cylindrical vortex generators," *Appl. Therm. Eng.*, vol. 220, no. August 2022, 2023, doi: 10.1016/j.applthermaleng.2022.119720.

[14] Y. Fang, I. B. Mansir, A. Shawabkeh, A. Mohamed, and F. Emami, "Heat transfer, pressure drop, and economic analysis of a tube with a constant temperature equipped with semi-circular and teardrop-shaped turbulators," *Case Stud. Therm. Eng.*, vol. 33, no. March, p. 101955, 2022, doi: 10.1016/j.csite.2022.101955.

[15] H. Sun, H. Fu, L. Yan, H. Ma, Y. Luan, and F. Magagnato, "Numerical Investigation of Flow and Heat Transfer in Rectangular Microchannels with and without Semi-Elliptical Protrusions," *Energies*, vol. 15, no. 13, 2022, doi: 10.3390/en15134927.

[16] [A. Alizadeh *et al.*, "Numerical investigation of the effect of the turbulator geometry (disturber) on heat transfer in a channel with a square section," *Alexandria Eng. J.*, vol. 69, pp. 383–402, 2023, doi: 10.1016/j.aej.2023.02.003.

[17] S. B. Kim, K. A. Moon, B. H. An, K. H. Choi, and H. U. Choi, "Experimental performance evaluation of air-based photovoltaic–thermal collector with rectangular turbulators and longitudinal fins," *Energy Reports*, vol. 12, no. June, pp. 1315–1324, 2024, doi: 10.1016/j.egyr.2024.07.038.

[18] C. C. Liao, W. K. Li, and H. E. Lin, "Heat transfer enhancement in microchannel systems through geometric modification of vortex generators and nanofluid integration: A numerical study," *Results Eng.*, vol. 25, no. January, p. 104138, 2025, doi: 10.1016/j.rineng.2025.104138.

[19] Y. Xi and F. Meng, "Numerical study on flow and heat transfer characteristics of rectangular mini-channel of interpolated double Sturbulators," *PLoS One*, vol. 19, no. 2 February, pp. 1–20, 2024, doi: 10.1371/journal.pone.0297678.

[20] B. Mei *et al.*, "Numerical investigation on

thermal-fractional characteristics inside a heated tube enhanced with a novel grooved cone turbulator," *Case Stud. Therm. Eng.*, vol. 66, no. January, p. 105712, 2025, doi: 10.1016/j.csite.2024.105712.

[21] P. Bhandari, D. Padalia, L. Ranakoti, R. Khargotra, K. András, and T. Singh, "Thermo-hydraulic investigation of open micro prism pin fin heat sink having varying prism sides," *Alexandria Eng. J.*, vol. 69, pp. 457–468, 2023, doi: https://doi.org/10.1016/j.aej.2023.02.016.

[22] T. R. KARAKUS *et al.*, "Experimental Investigation of Thermal Performance and Entropy Analysis of Sphere Turbulators," *Therm. Sci.*, vol. 29, no. 1, pp. 117–129, 2025, doi: 10.2298/TSCI240304165K.

[23] M. Bayat *et al.*, "Entropy and energy analysis of water/silver nanofluid flow in a microchannel by changing the angle of attack of a cam-shaped vortex generator," *Int. J. Thermofluids*, vol. 23, no. June, p. 100719, 2024, doi: 10.1016/j.ijft.2024.100719.

[24] A. Z. Dellil, A. Azzi, and B. A. Jubran, "Turbulent flow and convective heat transfer in a wavy wall channel," vol. 40, pp. 793–799, 2004, doi: 10.1007/s00231-003-0474-4.

[25] L. Zhang and D. Che, "Influence of corrugation profile on the thermalhydraulic performance of cross-corrugated plates," *Numer. Heat Transf. Part A Appl.*, vol. 59, no. 4, pp. 267–296, 2011, doi: 10.1080/10407782.2011.540963.

[26] [26] M. Bashi, S. Rashidi, and J. A. Esfahani, "Exergy analysis for a plate-fin triangular duct enhanced by a porous material," *Appl. Therm. Eng.*, vol. 110, pp. 1448–1461, 2017, doi: 10.1016/j.applthermaleng.2016.09.068.

[27] A. Bejan, "Entropy generation minimization: The new thermodynamics of finite-size devices and finite-time processes," *J. Appl. Phys.*, vol. 79, no. 3, pp. 1191–1218, 1996, doi: 10.1063/1.362674.

[28] F. A. Kline, S. J., and McClintock, "Describing Uncertainties in Single Sample Experiments," *Kline, S. J., McClintock, F. A.*, vol. 75, pp. 3–8, 1955.

[29] Y. Asako and Y. Yamaguchi, "Numerical Prediction of Transitional Characteristics of Flow and Heat Transfer in a," vol. 119, no. February 1997, pp. 3–10, 2016.

[30] J. Blazek, *Computational fluid dynamics: principles and applications*. Butterworth-Heinemann, 2015.
M. A. Ahmed, S. M. Hatem, and I. K. Alabdaly, "Investigation of Heat Transfer Enhancement and Entropy Increment in a U Channel with V-shaped Ribs for Improved Hydrothermal Performance," *Int. J. Heat Technol.*, vol. 42, no. 2, pp. 455–465, 2024, doi: 10.18280/ijht.420211.

[31] S. M. Vanaki and H. A. Mohammed, "Numerical study of nanofluid forced convection flow in channels using different shaped transverse ribs," *Int. Commun. Heat Mass Transf.*, vol. 67, pp. 176–188, Oct. 2015, doi: 10.1016/j.icheatmasstransfer.2015.07.004.